



HAL
open science

Rock salt behavior: From laboratory experiments to pertinent long-term predictions

M. Azabou, Ahmed Rouabhi, Laura Blanco Martín, F. Hadj-Hassen, M. Karimi-Jafari, G. Hévin

► **To cite this version:**

M. Azabou, Ahmed Rouabhi, Laura Blanco Martín, F. Hadj-Hassen, M. Karimi-Jafari, et al.. Rock salt behavior: From laboratory experiments to pertinent long-term predictions. *International Journal of Rock Mechanics and Mining Sciences*, 2021, 142, pp.104588. 10.1016/j.ijrmms.2020.104588. hal-03220133

HAL Id: hal-03220133

<https://minesparis-psl.hal.science/hal-03220133>

Submitted on 9 May 2023

HAL is a multi-disciplinary open access archive for the deposit and dissemination of scientific research documents, whether they are published or not. The documents may come from teaching and research institutions in France or abroad, or from public or private research centers.

L'archive ouverte pluridisciplinaire **HAL**, est destinée au dépôt et à la diffusion de documents scientifiques de niveau recherche, publiés ou non, émanant des établissements d'enseignement et de recherche français ou étrangers, des laboratoires publics ou privés.



Distributed under a Creative Commons Attribution - NonCommercial 4.0 International License

Rock salt behavior: From laboratory experiments to pertinent long-term predictions

M. Azabou^{a,*}, A. Rouabhi^a, L. Blanco-Martín^a, F. Hadj-Hassen^a, M. Karimi-Jafari^b, G. Hévin^c

^a*MINES ParisTech, PSL Research University, Centre de Géosciences, 35 rue St Honoré 77300 Fontainebleau, France*

^b*Geostock Entrepose, 2 rue des Martinets, Rueil-Malmaison, 92500, France*

^c*Storengy, 12 rue Raoul Nordling, Bois-Colombes, 92274, France*

Abstract

In the energy transition context, salt caverns are probably the most promising storage solution that promotes the development of intermittent renewable energies, due to their flexible and high deliverability. However, their design is still challenging since it should account for their entire lifetime, from rapid cycling exploitation to centuries of abandonment. The key to an optimal design is a constitutive model for rock salt that ensures pertinent short and long-term predictions. In this paper, we confront the results of five experimental campaigns conducted on different salts with existing rheological models. This confrontation proved that the studied models are capable of describing laboratory tests, however their predictions for the long term are either too conservative or overly optimistic. In practice, conservative or optimistic approaches do not ensure the optimal design of the facility. For this reason, we propose a new constitutive model that provides pertinent long-term predictions while interpreting satisfactorily short-term and long-term laboratory tests.

Keywords: rock salt, constitutive modeling, long-term creep, laboratory tests, time extrapolation

*Corresponding author

Email address: mejda.azabou@mines-paristech.fr (M. Azabou)

Preprint submitted to International Journal of Rock Mechanics and Mining Sciences November 13, 2020

1. Introduction

Solution mined caverns in salt formations have proven to be among the most efficient techniques for storage of different energy vectors since the 1960s (Bays, 1963; Ozarslan, 2012; Bai et al., 2014; Iordache et al., 2014; Lord et al., 2014; Michalski et al., 2017; Tarkowski and Czapowski, 2018; Firme et al., 2019; Soubeyran et al., 2019; Lankof and Tarkowski, 2020). Today these facilities have an important role in the energy transition context. Their flexible and high deliverability makes them the most promising solution to respond to peak demand for intermittent clean energies. The feasibility studies and the design of these caverns should account for the exploitation phase and for the decades and sometimes centuries of the abandonment phase. The optimal design of these structures rests upon the use of a constitutive model with pertinent short and long-term predictions.

There cannot be a unique rheological model able to describe the behavior of a geological material such as rock salt, under all kinds and within all ranges of thermo-mechanical loadings. What is sought instead, are approximate laws that can provide a close enough description to the real behavior of the rock within a given range of loading conditions. This explains the abundance of rock salt constitutive models in the literature. All the existing models, despite the differences in the phenomena they account for (dilatancy, healing, inverse creep, transient, steady state and tertiary creep, damage, extension, strain under tensile loading...), agree on two facts: first, rock salt has a strongly time dependent behavior and second, laboratory tests are essential for their parameters calibration. The multitude of models proves their limitations and justifies the need for the research on rock salt rheology to continue.

Long-term behavior is one of the main challenges for the rheological modeling of rock salt. In fact, it is technically possible to conduct tests under all desired loading conditions (different strain rates, temperatures, mechanical and thermal cycling...). However, contrary to the thermo-mechanical variables, we do not have control over the time of laboratory experiments, which is negligible compared to the lifetime of the underground facilities (a few months or years in the best case scenario, compared to few decades or even centuries in the field). When performing a time-extrapolation of the existing models, three kinds of

40 responses are obtained: (i) a transient response where the strain rate continuously decreases
 41 (Tijani et al., 1983; Labaune et al., 2018; Rouabhi et al., 2019), (ii) a purely steady-state
 42 response where the strain rate remains constant and the strain increases linearly over time
 43 (Odqvist, 1966) and (iii) a transient response that stabilizes into a steady-state regime where
 44 the strain starts increasing linearly over time (Munson and Dawson, 1981; DeVries et al.,
 45 2002; Heusermann et al., 2003; Bérest et al., 2007; Hampel, 2012; Nazary Moghadam et al.,
 46 2013; Wolters et al., 2012; Günther et al., 2015; Khaledi et al., 2016; Deng et al., 2020; Wu
 47 et al., 2020).

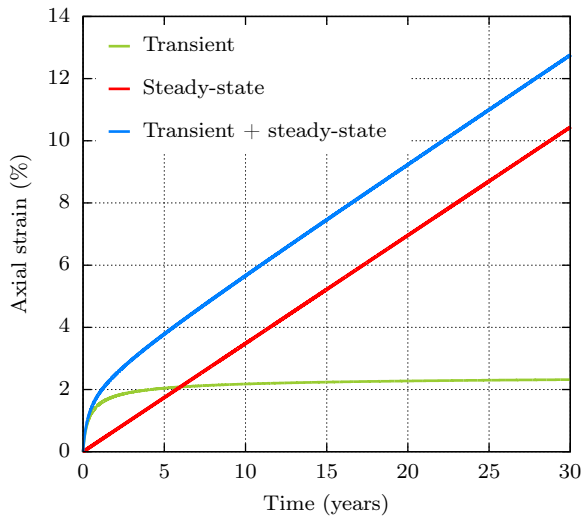


Figure 1: Time-extrapolation of three models with different creep responses on a uniaxial creep test.

48 Figure 1 illustrates this point where we show a qualitative comparison of the three
 49 responses based on the simulation of a uniaxial creep test over 30 years. As shown, the
 50 transient model gives an overly optimistic prediction while the two other models are rather
 51 conservative. Bérest et al. (2008) studied the differences in the long-term behavior predicted
 52 by these types of models. The study confirmed that the transient models and the steady
 53 state ones predict significantly different behaviors on the long term, and suggested that,
 54 since in terms of laboratory tests both models give satisfactory interpretations, the most
 55 conservative predictions should be selected. However in practice, the optimal design of salt
 56 caverns cannot be based on overly conservative approaches.

57 The purpose of this paper is to propose a model with pertinent predictions for long-term
58 creep behavior. We propose an enrichment to the distortion part of a model that has been
59 detailed in (Rouabhi et al., 2019). The modification consists in adding to the transient
60 component, a second transient mechanism inspired by the Munson-Dawson (Munson and
61 Dawson, 1981) transient creep. This allows to have a compromise between the steady state
62 models and the transient ones in terms of the strain rate and the characteristic time. The
63 added mechanism allows also to describe inverse creep (Julien, 1999; Heusermann et al.,
64 2003; Karimi-Jafari, 2007; Günther et al., 2015; Labaune, 2018; Gharbi et al., 2020) and
65 links it to hysteresis loops of the unloading-loading cycles of triaxial compression tests. The
66 authors are aware that in-situ data that covers years of exploitation activity, is needed to
67 fully validate the model and truly assess the pertinence of its time extrapolation. However,
68 acquiring such data and using it for research work is difficult, since -even if they exist- these
69 measurements are destined for exploitation purposes.

70 This paper is structured as follows. In the first section two existing models and the new
71 proposed one are presented. In section 3, we compare these constitutive laws on the basis
72 of five experimental campaigns conducted at Mines ParisTech on rock salts from different
73 geographic locations. The comparison concerns the capability of the three models to fit
74 long-term (creep) and short-term (conventional triaxial compression) tests with the same
75 parameter set, and the pertinence of their long-term predictions. In section 4 the new
76 model is used to analyze a comprehensive test campaign and the inverse creep phenomenon
77 is discussed in section 5.

78 2. Constitutive models

79 All these constitutive laws agree on the partition of the total strain rate tensor $\underline{\dot{\underline{\epsilon}}}$ into
 80 elastic $\underline{\dot{\underline{\epsilon}}}_{\text{el}}$, thermal $\underline{\dot{\underline{\epsilon}}}_{\text{th}}$ and viscoplastic parts $\underline{\dot{\underline{\epsilon}}}_{\text{vp}}$:

$$\underline{\dot{\underline{\epsilon}}} = \underline{\dot{\underline{\epsilon}}}_{\text{el}} + \underline{\dot{\underline{\epsilon}}}_{\text{th}} + \underline{\dot{\underline{\epsilon}}}_{\text{vp}} \quad ; \quad \underline{\dot{\underline{\epsilon}}}_{\text{el}} = \frac{1 + \nu}{E} \underline{\dot{\underline{\sigma}}} - \frac{\nu}{E} \text{tr}(\underline{\dot{\underline{\sigma}}}) \underline{\underline{1}} \quad ; \quad \underline{\dot{\underline{\epsilon}}}_{\text{th}} = \alpha_{\text{th}} \dot{T} \underline{\underline{1}} \quad (1)$$

81 where E, ν are the elastic constants, $\underline{\underline{\sigma}}$ is the Cauchy stress tensor, $\underline{\underline{1}}$ is the unit tensor,
 82 α_{th} is the linear thermal expansion coefficient and T is the temperature. The viscoplastic
 83 strain tensor is generally given as a function of the thermodynamic state $(\underline{\underline{\sigma}}, T)$ and internal
 84 variables ξ with a rate that depends on $\underline{\underline{\sigma}}, T$ and the internal variables:

$$\underline{\dot{\underline{\epsilon}}}_{\text{vp}} = \underline{\underline{\mathcal{F}}}(\underline{\underline{\sigma}}, T, \xi), \quad \dot{\xi} = \underline{\underline{\mathcal{G}}}(\underline{\underline{\sigma}}, T, \xi) \quad (2)$$

85 it is on the definitions of ξ , $\underline{\underline{\mathcal{F}}}$ and $\underline{\underline{\mathcal{G}}}$ that those models differ. In this section we present the
 86 following models: Munson-Dawson, Lemaitre and the model developed in this work that we
 87 shall call RTL.

88 2.1. The Munson-Dawson constitutive model

89 This model has been detailed in (Munson and Dawson, 1981) and it states the following

$$\underline{\dot{\underline{\epsilon}}}_{\text{vp}} = F \underline{\dot{\underline{\epsilon}}}_{\text{ss}} \quad ; \quad \underline{\dot{\underline{\epsilon}}}_{\text{ss}} = \dot{\underline{\underline{J}}} = \dot{\underline{\underline{\epsilon}}}_{\text{ss}}(\underline{\underline{\sigma}}, T) \underline{\underline{J}} \quad ; \quad \underline{\underline{J}} = \underline{\underline{\sigma}}' / \|\underline{\underline{\sigma}}'\| \quad (3)$$

91 where $\underline{\underline{\sigma}}'$ is the deviatoric part of the Cauchy stress tensor ($\underline{\underline{\sigma}}' = \underline{\underline{\sigma}} - \frac{1}{3} \text{tr}(\underline{\underline{\sigma}}) \underline{\underline{1}}$), $\underline{\dot{\underline{\epsilon}}}_{\text{ss}}$ denotes
 92 the steady state strain rate tensor and F is defined as follows

$$F = \begin{cases} \exp(\Delta(1 - \zeta/\varepsilon_t^*)^2) & \text{if } \zeta \leq \varepsilon_t^* \\ \exp(-\delta(1 - \zeta/\varepsilon_t^*)^2) & \text{if } \zeta \geq \varepsilon_t^* \end{cases} \quad (4)$$

$$\dot{\zeta} = (F - 1) \dot{\underline{\underline{\epsilon}}}_{\text{ss}} \quad (5)$$

94 In this work we assume the following

$$\dot{\underline{\underline{\epsilon}}}_{\text{ss}}(\underline{\underline{\sigma}}, T) = A \exp\left(A_M \left(\frac{1}{T_r} - \frac{1}{T}\right)\right) \langle G \rangle^n \quad ; \quad \varepsilon_t^* = K_0 e^{cT} q^m \quad (6)$$

95 where G is a loading function chosen as $G = q$, with q the von mises equivalent stress, $\langle \cdot \rangle$
 96 are the Macaulay brackets, i.e., $\langle x \rangle = (x + |x|)/2$, T_r is the reference temperature, A , A_M , n ,
 97 c , K_0 , m , Δ and δ are material constants. We note that this model accounts for transient
 98 creep (via the function F) that saturates at ε_t^* and the steady state flow $\dot{\varepsilon}_{ss}$ takes over.

99 2.2. The Lemaitre constitutive model

100 This model assumes that rock salt creep is a purely transient flow, the viscoplastic strain
 101 rate decreases asymptotically to zero. It states the following

$$\dot{\underline{\underline{\varepsilon}}}_{vp} = \sqrt{3/2} \dot{\gamma}_{vp} \underline{J} \quad (7)$$

102 where γ_{vp} is the viscoplastic distortion defined as

$$\dot{\gamma}_{vp} = \gamma_{vp}(\underline{\underline{\sigma}}, T, \gamma_{vp}) = \alpha \exp(A_L(\frac{1}{T_r} - \frac{1}{T})) \left\langle \frac{G}{K} \right\rangle^{\beta/\alpha} \gamma_{vp}^{1-\frac{1}{\alpha}} \quad (8)$$

103 α , β , A_L and K and positive rheological constants and T_r the reference temperature. Sim-
 104 ilarly to the previous model, G is a loading function $G = G(\underline{\underline{\sigma}}, T, \gamma_{vp})$ and is chosen as
 105 $G = q$.

106 2.3. The RTL2020 constitutive model

107 Similar to the model detailed in [Rouabhi et al. \(2019\)](#), for the viscoplastic strain rate
 108 tensor, RTL assumes the following

$$\dot{\underline{\underline{\varepsilon}}}_{vp} = \sqrt{\frac{3}{2}} \dot{\gamma}_{vp} \underline{N} - \frac{1}{\sqrt{3}} \dot{\zeta}_{vp} \underline{I} \quad (9)$$

109 where $\dot{\zeta}_{vp} = -tr(\dot{\underline{\underline{\varepsilon}}}_{vp})$ and $\dot{\gamma}_{vp} = \sqrt{2/3} \|\dot{\underline{\underline{\varepsilon}}}'_{vp}\|$ are the rates of the volumetric strain and the
 110 viscoplastic distortion, respectively, \underline{N} is a unit tensor defining the deviatoric flow direction
 111 and $\underline{I} = \underline{1}/\sqrt{3}$. The general formalism of the viscoplastic distortion is defined as

$$\dot{\gamma}_{vp} = \dot{\gamma}_L + \dot{\gamma}_R \quad ; \text{ with } \begin{cases} \dot{\gamma}_L = \psi_L(\underline{\underline{\sigma}}, T, \gamma_L) \\ \dot{\gamma}_R = \psi_R(\underline{\underline{\sigma}}, T, \gamma_R) \end{cases} \quad (10)$$

112 here $\dot{\gamma}_L$ describes a transient creep mechanism of Lemaitre's type, and $\dot{\gamma}_R$ is an added
 113 transient mechanism inspired by the Munson-Dawson model. The first transient mechanism
 114 is defined by

$$\psi_L(\underline{\sigma}, T, \gamma_L) = \alpha \exp\left(A_R\left(\frac{1}{T_r} - \frac{1}{T}\right)\right) \left\langle \frac{G}{A_2} \right\rangle^{n_2} \gamma_L^{1-\frac{1}{\alpha}} \quad (11)$$

115 where α , A_R , A_2 and n_2 are material parameters, G is a loading function. The added
 116 distorsion mechanism γ_R is defined as

$$\psi_R(\underline{\sigma}, T, \gamma_R) = \begin{cases} A(1 - \gamma_R/\bar{\gamma}_R)^n R(\underline{\sigma}, T) & \text{if } \gamma_R \leq \bar{\gamma}_R \\ -B(\gamma_R/\bar{\gamma}_R - 1)^m R(\underline{\sigma}, T) & \text{if } \gamma_R \geq \bar{\gamma}_R \end{cases} ; \quad \bar{\gamma}_R = \bar{\gamma}_R(\underline{\sigma}, T) \quad (12)$$

117 here A , B , m and n are material parameters such that $A > 0$, $B > 0$ and $m > 1$, $n > 1$.

118 The model offers enough flexibility in the choice of the functions ψ_L , $\bar{\gamma}_R$ and R . In this work
 119 we have made the following considerations:

- 120 • $\dot{\gamma}_L$ corresponds to the viscoplastic distorsion of Lemaitre model $\dot{\gamma}_{vp}$;
- 121 • $\bar{\gamma}_R$ is considered to be analogue to the saturation value ε_t^* in Munson-Dawson model,
 122 it is given by

$$\bar{\gamma}_R = \left\langle \frac{G}{A_1} \right\rangle^{n_1} \quad (13)$$

123 where A_1 and n_1 are material parameters.

- 124 • As for the definition of the function R , it is considered to be the same as ψ_L in order
 125 to link the two mechanisms and ensure that their contributions have the same order
 126 of magnitude

$$R(\underline{\sigma}, T) = \exp\left(A_R\left(\frac{1}{T_r} - \frac{1}{T}\right)\right) \left\langle \frac{G}{A_2} \right\rangle^{n_2} \quad (14)$$

- 127 • We chose the loading function G such that $G = q$.

128 As for the volumetric viscoplastic strain, it remains unchanged from the definition given in
 129 RTL (Rouabhi et al., 2019) as

$$\dot{\zeta}_{vp} = \phi(\underline{\sigma}, T, \gamma_{vp}) \dot{\gamma}_{vp} = z \frac{\langle p/N_z \rangle^{n_z} - \gamma_{vp}}{\langle p/M_z \rangle^{m_z} + \gamma_{vp}} \dot{\gamma}_{vp} \quad (15)$$

130 where z, N_z, n_z, M_z and m_z are material parameters and p is the mean pressure ($p = -tr(\underline{\sigma})/3$).
 131 We note that the RTL model is equivalent to the Munson Dawson model when the following
 132 considerations are made:

- 133 • the parameter α from equation 11 is set to 1;
- 134 • the parameter A from equation 12 is taken as $A = \exp(\Delta)$;
- 135 • the parameter n from equation 12 is linked to the parameter Δ via the following
 136 equation

$$n = \begin{cases} -0.0098\Delta^3 + 0.2040\Delta^2 + 0.5622\Delta + 2.0252 & \text{when } \Delta \leq 6 \\ 1.9987\Delta - 1.4567 & \text{when } \Delta > 6 \end{cases} \quad (16)$$

- 137 • $B = \delta = 0$ (equations 4 and 12).

138 The advantage of the mechanism γ_R in this model is that it can be easily integrated com-
 139 pared to the exponential formulation used in Munson-Dawson. Under constant stress and
 140 temperature, the analytical solution for equation 11 can be written as

$$\gamma_R(t) = \gamma_{R0} + (\bar{\gamma}_R - \gamma_{R0})\xi \quad (17)$$

141 where ξ is given by

$$\xi(t) = 1 - \left(\frac{1}{1 + V(t - t_0)} \right)^{\frac{1}{k-1}} \quad (18)$$

142 with

$$V = (k - 1)U \frac{A_1^{n_1}}{A_2^{n_2}} q^{n_2 - n_1} \quad (19)$$

143 When $\gamma_R \leq \bar{\gamma}_R$ we have: $k = n$, $U = A(1 - \gamma_{R0}/\bar{\gamma}_R)^{n-1}$ and if $\gamma_R \geq \bar{\gamma}_R$ then $k = m$,
 144 $U = B(\gamma_{R0}/\bar{\gamma}_R - 1)^{m-1}$.

145 In Figure 2 we illustrate the role of each of the parameters $A, B, n, m, A_1, n_1, A_2$ and n_2 . We
 146 start from the parameter set given in Table 1 and in each case one parameter is varied, the
 147 simulated scenario is one of a uniaxial creep test were the axial stress (q in this case) is held
 148 constant at 10 MPa during 15 days and then dropped to 5 MPa for another 15 days. In

149 the plots we present the evolution of the distortion γ_R in time and the value of $\bar{\gamma}_R$ in each
 150 deviatoric stage (recall that $\bar{\gamma}_R = \left(\frac{q}{A_1}\right)^{n_1}$).

A	B	n	m	A_1	n_1	A_2	n_2
0.5	0.05	5	5	0.3	3	0.5	4

Table 1: Initial parameter set used to study the role of the parameters of the distortion mechanism γ_R (the unit system is such that strain is in $\mu\text{m}/\text{m}$, stress is in MPa and time in days).

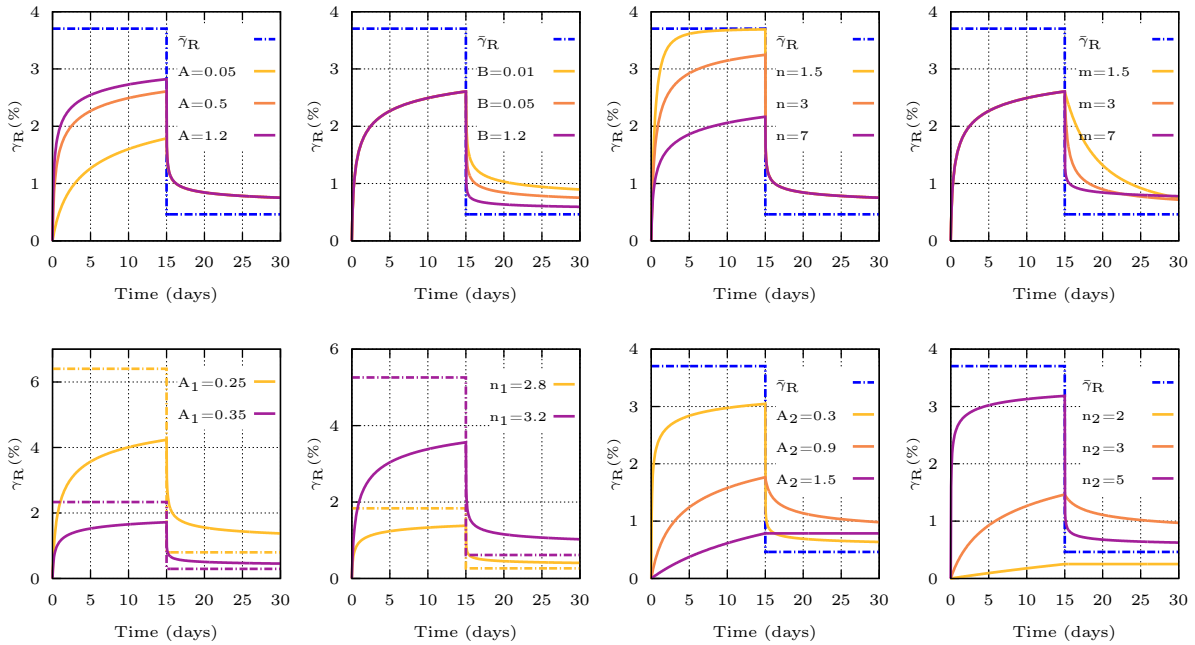


Figure 2: Effect of the parameters of the distortion mechanism γ_R in RTL model, predictions of a multistage creep test, note that in the sub-figures describing the effects of parameters A_1 and n_1 , the value of $\bar{\gamma}_R$ corresponding to each parameter is plotted in the same color in dashed line.

151 The parameters A , B , n and m affect the rate at which γ_R tends to $\bar{\gamma}_R$ as shown in the
 152 four top sub-figures of Figure 2. Particularly after a load drop, the parameters B and m
 153 affect the duration of the observed transient flow. The four sub-figures in the bottom of
 154 Figure 2 show that the mechanism is more sensitive to the parameters defining $\bar{\gamma}_R$ (A_1 and
 155 n_1) and to A_2 and n_2 . As shown in Figure 2, the parameters of the γ_R distortion mechanism

156 give the model a great flexibility to fit different experimental responses.

157 **3. Models comparison on the basis of laboratory tests**

158 *3.1. Laboratory tests*

159 We analyzed 5 experimental campaigns conducted at Mines ParisTech between 2012 and
160 2020 on salts from different locations (USA, Europe, Middle East), to which we will refer
161 as salt 1, salt 2, salt 3, salt 4 and salt 5. From each of the campaigns we chose a multistage
162 creep test (considered as a long-term test) and a conventional triaxial compression test
163 (short-term test). The tests of the first four campaigns were all conducted following the
164 same procedure (preconditioning, measurement techniques -strain gauges-, experimental set
165 up and the axial strain rate $\dot{\epsilon}_{ax}$ for the short-term tests). In addition, in these four series of
166 tests the confining pressure (P) is maintained constant during the creep tests and the changes
167 in the deviatoric stages are applied by modifying the axial stress (Q). However, for salt 5
168 the procedure for the short-term tests was slightly different (duration and confining pressure
169 for specimen preconditioning, measurement techniques -radial extensometer and global axial
170 displacement-, axial strain rate). Also the creep test on this salt lasted significantly longer
171 compared to the creep tests from the first four campaigns and it differs from them in the
172 testing procedure: the deviatoric stages are obtained by varying both the axial and lateral
173 stresses such that the mean pressure $(Q + 2P)/3$ is held constant at 10 MPa throughout the
174 test.

175 *3.2. Parameters fitting and time extrapolation*

176 For each salt, the results are analyzed with the three models (Munson-Dawson, Lemaitre
177 and RTL) and the best fitting obtained (with the same parameter set for each model) is
178 provided. Afterwards, these parameters are used to perform a time extrapolation of the
179 models on a virtual scenario of a uniaxial creep test of 10000 days.

180 In the three models we are studying, the temperature effect is given by the Arrhenius law,
181 and all the creep tests we are analyzing in this section are carried out at constant temper-
182 ature. For this reason, we have set the parameters $A_M = A_L = A_R = 1725$ K, also the

183 reference temperature T_r was set to 289 K. In addition, since the stages of deviatoric stress
184 in all the creep tests are ascending, the parameter B from equations 12 was set to 0 and
185 therefore the parameter m was not adjusted. Figures 3 to 7 show the fittings of the three
186 models on the tests from the five campaigns and the results of the time extrapolation. In
187 each of these figures, the top graph represents the analysis of a triaxial compression test (at
188 a constant confining pressure and a constant strain rate that are specified on the graph), the
189 middle graph corresponds to a multistage creep test (the test temperature and conditions
190 are indicated on the graph) and the bottom figure is a time extrapolation of the three models
191 for a uniaxial creep test at $T = 40^\circ$ C. The fitting parameters are provided in Table 2.

192 We can see that the three models give satisfactory interpretations to both the short-term
193 and the long-term tests, they are all able to describe the behavior of rock salt at the labo-
194 ratory scale for this specific type of tests (time and loading ranges). As for the long-term
195 predictions, the transient creep phase described by Munson-Dawson model is practically
196 inexistent compared to the steady state flow and it has the same time span of laboratory
197 tests durations (a few days), the time extrapolation of this model is rather conservative since
198 the steady state flow is dominant and the strain increases linearly over time. However, the
199 Lemaitre model is overly optimistic as it assumes that the strain rate keeps on decreasing
200 infinitely and the strain almost tends to stabilize. On the other hand, in all the studied cases
201 RTL gives predictions that are between these two extremes, the strain increases in time but
202 neither linearly nor with an almost-zero rate. Besides, in RTL time extrapolation we dis-
203 tinguish a characteristic time (for the mechanism γ_R) that is comparable to the duration of
204 the prediction.

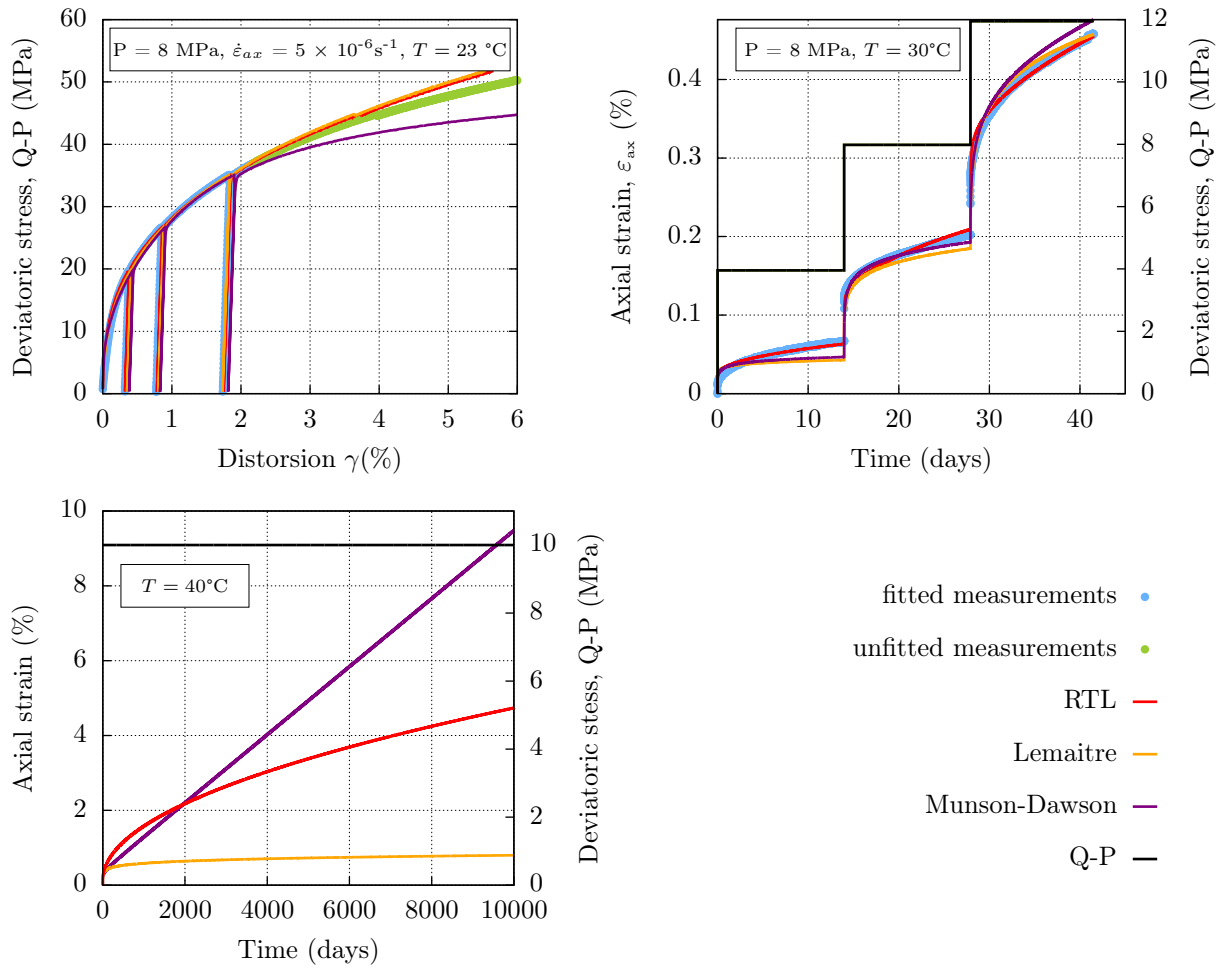


Figure 3: Fittings of tests on salt 1 and time extrapolation of the three fitted models.

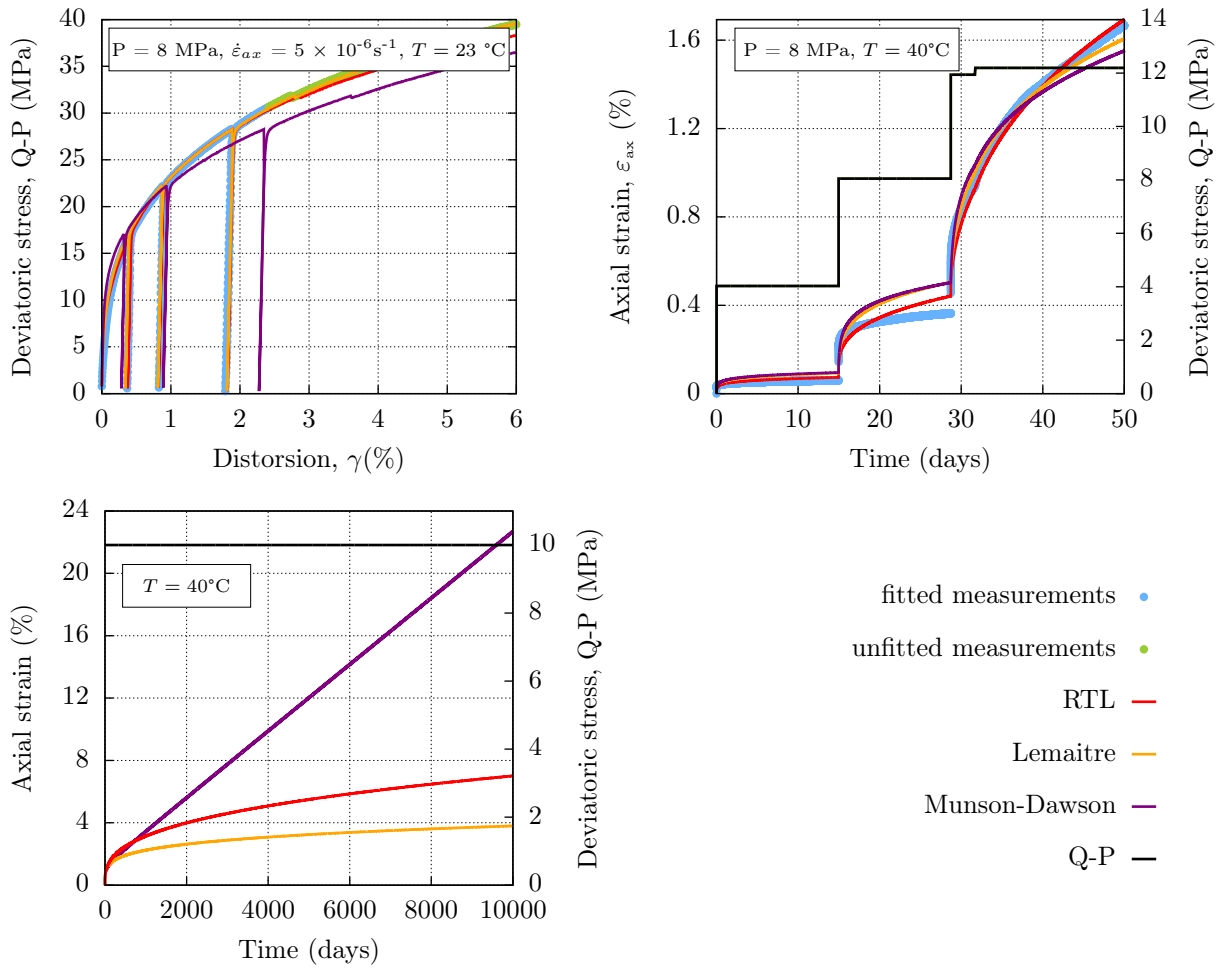


Figure 4: Fittings of tests on salt 2 and time extrapolation of the three fitted models.

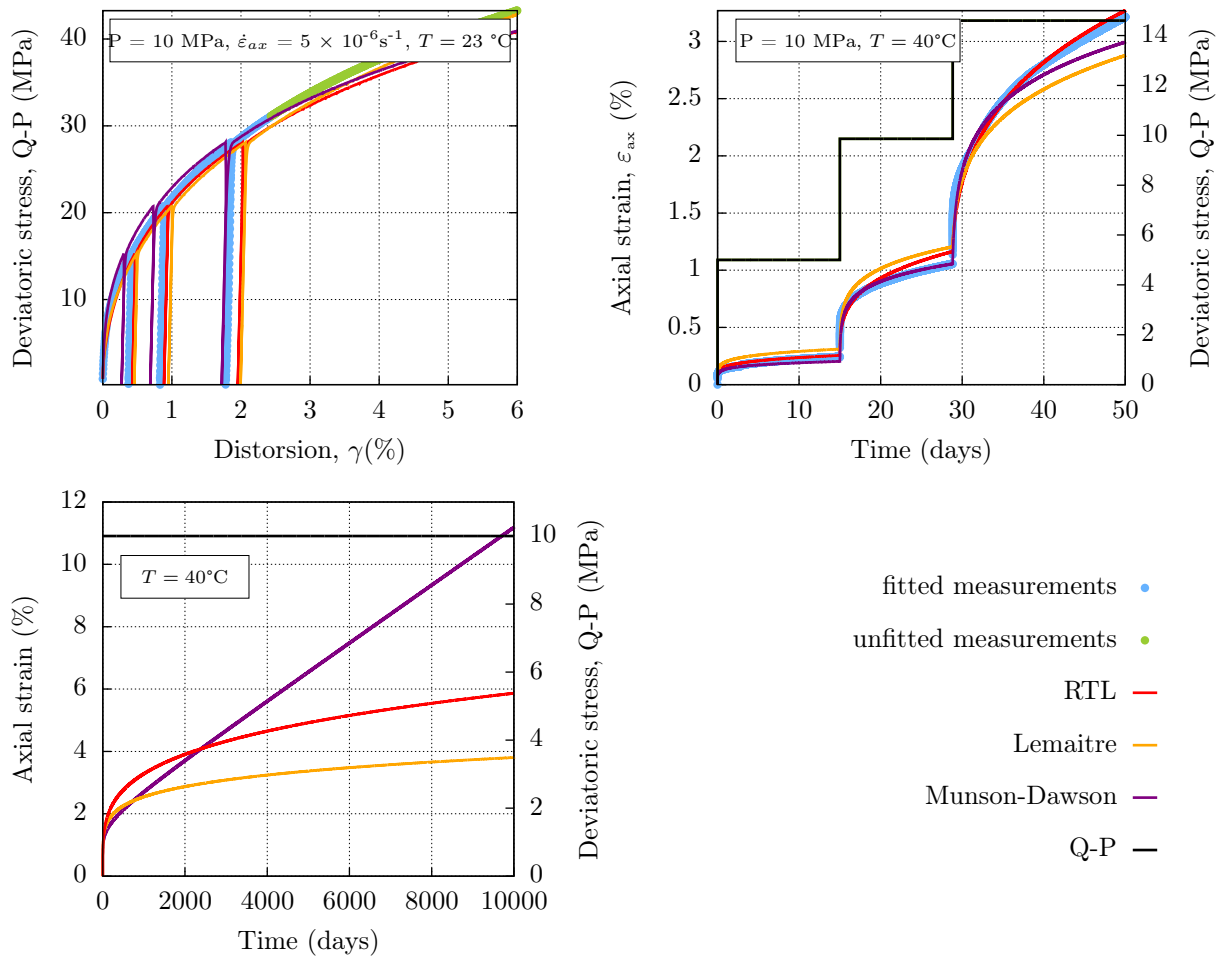


Figure 5: Fittings of tests on salt 3 and time extrapolation of the three fitted models.

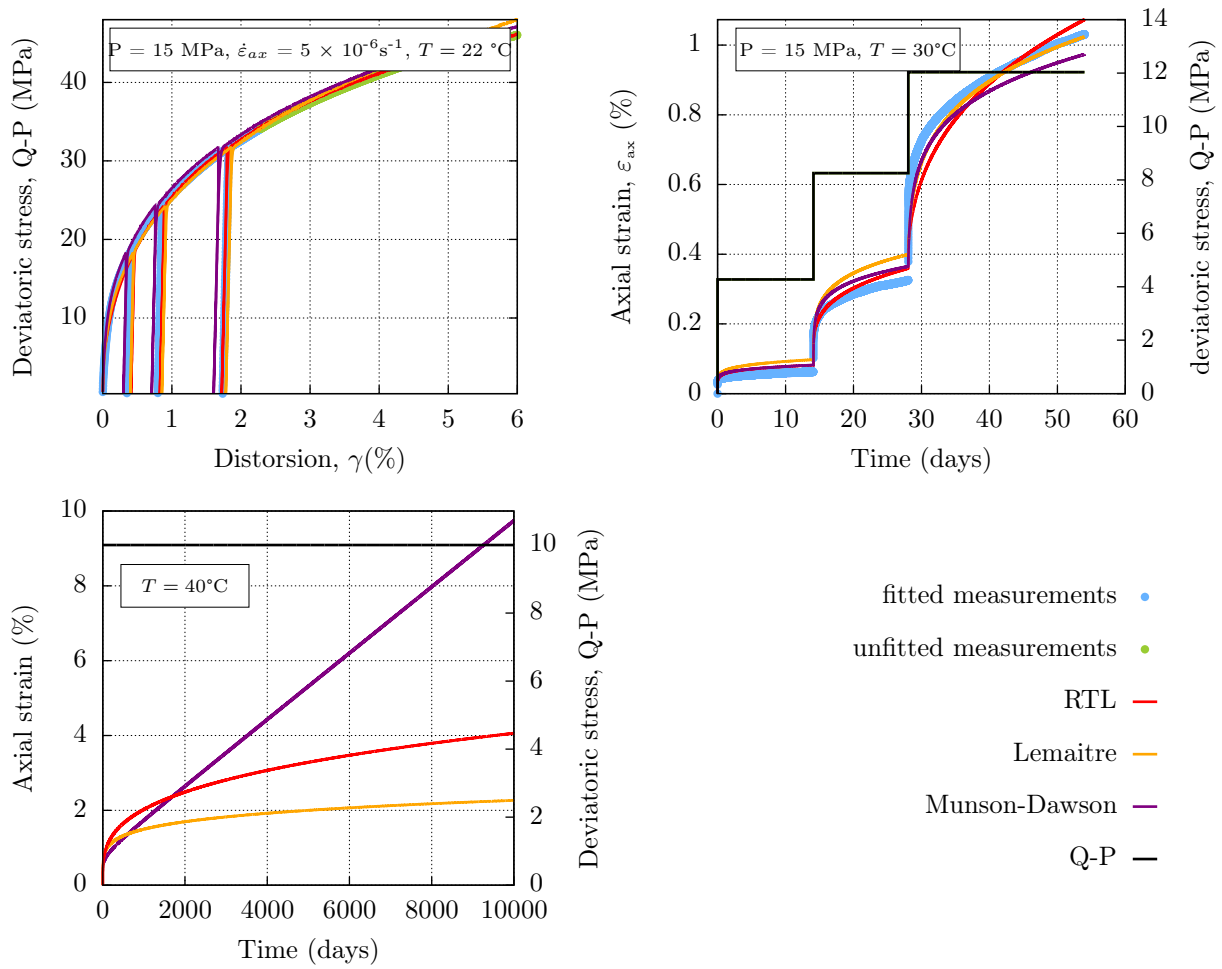


Figure 6: Fittings of tests on salt 4 and time extrapolation of the three fitted models.

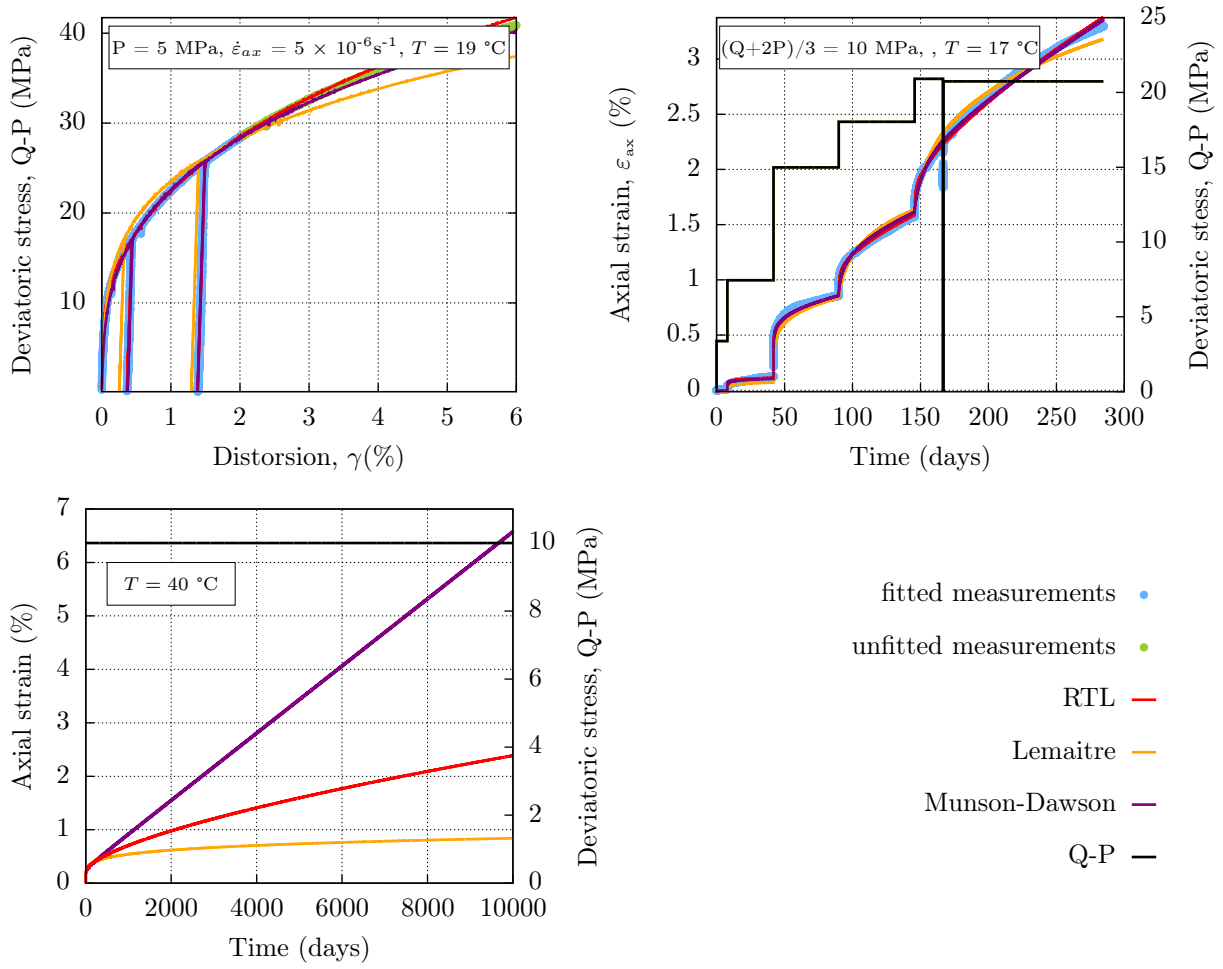


Figure 7: Fittings of tests on salt 5 and time extrapolation of the three fitted models.

Parameters	Salt 1	Salt 2	Salt 3	Salt 4	Salt 5
Elasticity					
E	29518	27499	28567	32172	22126
ν	0.32	0.32	0.30	0.31	0.2
Munson-Dawson					
A	4.636×10^{-8}	2.713×10^{-3}	0.5882	0.5513	4.46×10^{-4}
n	8.0975	3.7	1.	1.01	3.936
m	1.387	2.3	2.8075	2.6922	2.7062
K_0	159.5602	69.6769	31.2385	18.5017	5.8505
Δ	14.0464	9.3	11.1551	11.6182	15.3698
Lemaitre					
α	0.1363	0.2288	0.1746	0.1801	0.1904
β	2.4189	2.6356	2.0518	2.265	3.4854
K	0.4938	0.4832	0.16	0.3034	1.4091
RTL					
α	0.5072	0.3601	0.2601	0.3201	0.6709
A_1	0.4896	0.061	0.0181	0.04107	0.2937
n_1	2.5093	1.473	1.162	1.3711	2.2839
A_2	0.1916	1.0945	0.3986	0.868	4.5478
n_2	2.7967	9.2482	9.6768	9.1676	6.3023
A	36.055	6.81×10^{-3}	0.01	2.94×10^{-2}	684
n	11.5263	9.2644	13.5	12.11	8.8926

Table 2: Parameters used to fit the experimental data in Figures 3 to 7. The unit system is such that strain is in $\mu\text{m}/\text{m}$, stress is in MPa and time in days.

205 4. Analysis of a comprehensive testing campaign with RTL

206 In order to show the capabilities of RTL to fit simultaneously short and long-term tests,
207 with different and relatively complicated loading paths, we use this constitutive model to
208 analyze a comprehensive testing campaign performed on specimens from salt 5 at Mines
209 ParisTech.

210 4.1. Laboratory tests

211 In addition to the triaxial compression and the creep tests shown in Figure 7, we con-
212 ducted the following tests on specimens from salt 5:

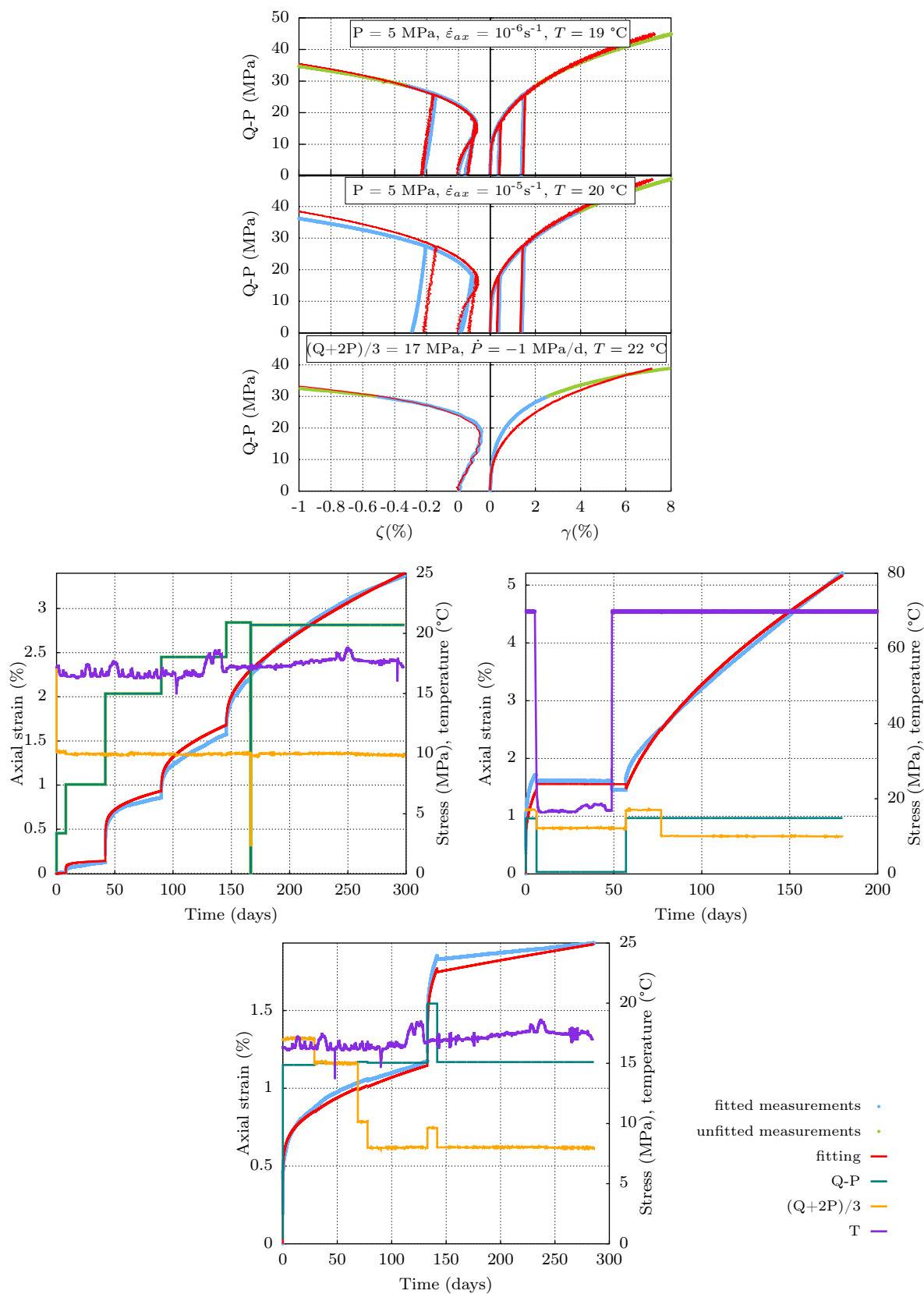
- 213 • a typical triaxial compression test under a confining pressure $P = 5$ MPa and an
214 constant axial strain rate of $\dot{\epsilon}_{ax} = 10^{-5} \text{ s}^{-1}$, performed at room temperature;
- 215 • a constant mean stress triaxial compression test, where the confining and the axial
216 pressures (respectively P and Q) vary with the respective rates of $\dot{P} = -1$ MPa/d and
217 $\dot{Q} = 2$ MPa/d in order to maintain a constant mean stress of $(Q + 2P)/3 = 17$ MPa
218 (at room temperature);
- 219 • a multistage creep test at room temperature, where the effect of the mean pressure is
220 investigated: during some of the stages the axial and lateral stresses are changed in
221 order to maintain a constant deviatoric stress and change the mean pressure;
- 222 • a multistage creep test similar to the last one, but performed at $T = 70$ °C.

223 This testing campaign is comprehensive as it includes tests with different and non-classic
224 loading paths, also all the creep tests last over 200 days.

225 4.2. Parameters fitting

226 Since some of the tests have different temperature stages, the parameters A_R and α_{th} were
227 fitted. The elastic parameters E and ν were fitted using the unloading/reloading cycles of
228 the triaxial compression tests. The remaining parameters were fitted in two independent
229 steps: those related to the deviatoric part and those related to the volumetric part. The

230 experimental measurements of the distortion were used to fit the volumetric strain part; this
231 ensures the independence of the two fittings. The fittings of the analyzed tests are given
232 in Figure 8 and the corresponding single parameter set in Table 3. As can be seen, RTL
233 allows a satisfactory matching to the experimental measurements and it describes correctly
234 the deviatoric and the volumetric behavior. The quality of the fittings shown in Figure 8
235 proves the robustness of RTL as a rock salt constitutive law.



20
 Figure 8: Fitting of three short-term tests (top) and three creep tests (bottom) with a single parameter set. Note that for the second creep test, an isothermal (room temperature), isotropic phase (at $(Q + 2P)/3 = 12 \text{ MPa}$) was applied.

Elasticity and Temperature effect								
E	ν	A_R	α_{th}					
22126	0.2	4457	3.27×10^{-5}					
Distorsion								
a	A_1	n_1	A_2	n_2	A	n	B	m
0.5812	0.1854	2.1012	3.7009	6.7562	155.6582	11.989	0.01918	2.2195
Dilatancy								
z	n_z	N_z	m_z	M_z				
0.4523	1.2644	0.0241	1.028	0.024				

Table 3: Parameters used to fit both short-term and creep tests on Landes salt (the unit system is such that strain is in $\mu\text{m}/\text{m}$, stress is in MPa and time in days).

236 5. Inverse creep

237 When the deviatoric stress level decreases during a classic creep test, the specimen's
238 length increases for a brief duration before it starts decreasing again. This phenomenon
239 assumes that the viscoplastic strain rate can be negative following a loading drop (inverse
240 creep). Observing this during classic creep tests is delicate due to its small magnitude and
241 brief duration. However this phenomenon is exhibited during the unloading-loading cycles
242 of classic triaxial compression tests, in fact we observed that during these tests the decrease
243 of the deviatoric stress comes with an irreversible strain and the creation of a hysteresis loop.
244 We select the first triaxial compression test and the third creep test presented in Figure 8,
245 we fit the two data sets with RTL and a single parameter set twice: the first fitting does
246 not allow a change in the direction of the viscoplastic strain (i.e., the parameter B is set to
247 0) and the second fitting is performed with $B \neq 0$. The results are respectively shown in
248 Figure 9 and 10 and the corresponding parameters are listed in Table 4.
249 Both fittings qualities are satisfactory, in Figure 9 the loading drop during the two analyzed
250 tests is purely elastic as it can be seen in the zoomed plots. However, activating the inverse
251 creep mechanism ($B \neq 0$) allows to describe the hysteresis loop observed during the short-
252 term test; it characterizes correctly the viscoplastic flow that comes with this unloading-

253 loading cycle. Also, following the load drop in the creep test, the model describes a very
 254 small and hardly distinguishable inverse creep: the strain rate decreases and then starts
 255 increasing again. We would like to highlight the fact that in the experimental measurements
 256 inverse creep was not observed, which is almost always the case during creep tests. This
 257 phenomenon has a very small order of magnitude (as predicted by the model in Figure 10),
 258 yet this fitting proves that it is directly linked to the loops of the unloading-loading cycles
 259 of triaxial compression tests. In Figure 11 we detail the fitting of the creep test in Figure 10
 260 and we explicit the contributions of the distortion mechanisms of RTL. We can see that
 261 following the load drop γ_R decreases and tends to the new $\bar{\gamma}_R$ but with a very small rate,
 262 which is why γ_L (steadily increasing) prevails and this results in a very discreet inverse creep
 263 phenomenon.

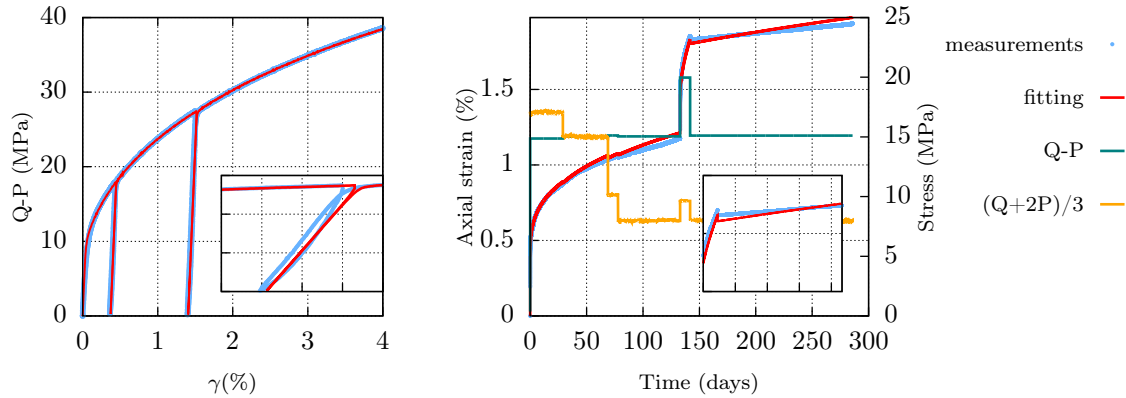


Figure 9: Fitting of a conventional triaxial test (left) and a multistage creep test (right) with a single parameter set without accounting for inverse creep.

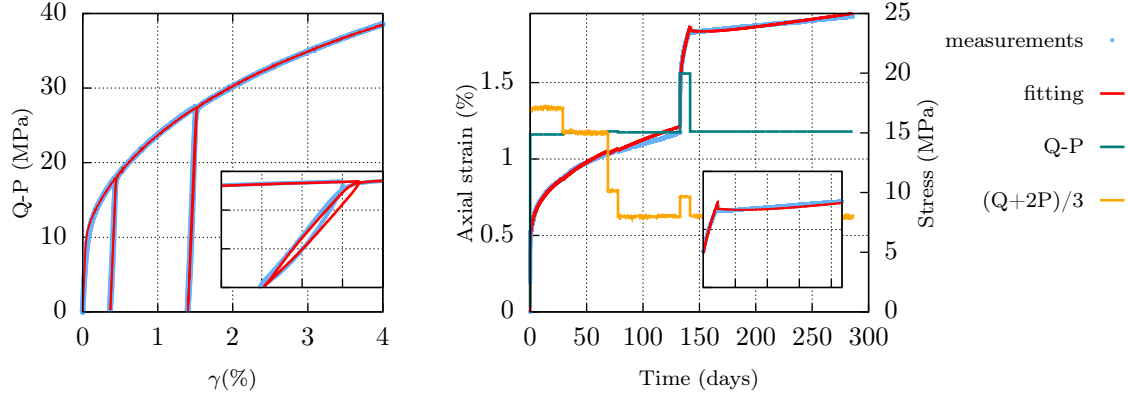


Figure 10: Fitting of a conventional triaxial test (left) and a multistage creep test (right) with a single parameter set accounting for inverse creep.

Elasticity and Temperature effect								
E	ν	A_R	α_{th}					
22126	0.2	4457	3.27×10^{-5}					
Distorsion without accounting for inverse creep								
a	A_1	n_1	A_2	n_2	A	n	B	m
0.5812	0.1854	2.1012	3.7009	6.7562	155.6582	12.11	0	–
Distorsion accounting for inverse creep								
a	A_1	n_1	A_2	n_2	A	n	B	m
0.3840	0.2136	2.0581	2.4199	9.9698	0.2223	12.11	3.72×10^{-5}	4.5795

Table 4: Parameters used for the fittings shown in Figures 9 to 11 (the unit system is such that strain is in $\mu\text{m}/\text{m}$, stress is in MPa and time in days)

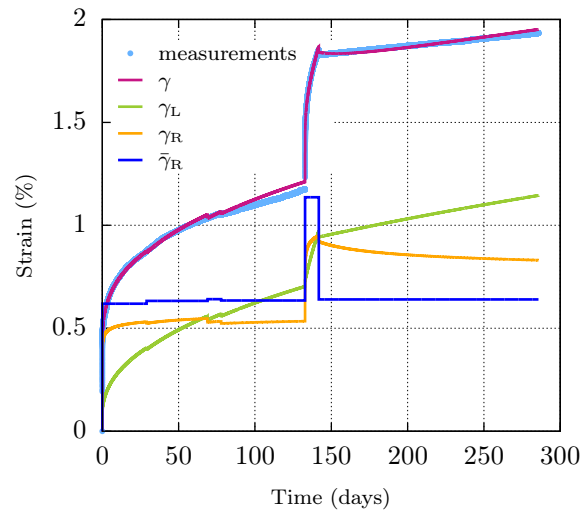


Figure 11: Fitting of a the multistage creep test shown in Figure 10 and detailing of the contributions of the distortion mechanisms in RTL.

264 **6. Conclusion**

265 In this paper we discussed the aptitude of rock salt constitutive models to provide per-
266 tinent short and long-term predictions, since they are crucial for the optimal design of salt
267 caverns. Our discussion was based on the confrontation of existing models with five ex-
268 perimental campaigns conducted on salts from different geographic locations. We found
269 that the studied models gave satisfactory interpretations to laboratory tests. However, their
270 long-term predictions were either too conservative or very optimistic. A new model was
271 developed and included in this confrontation. It also allowed correct interpretations for lab-
272 oratory tests but unlike the existing models, it gave pertinent predictions for the long term.
273 This new model was also tested against a comprehensive testing campaign that comprises
274 short-term, long-term and non-classic creep tests. It provided a valid fitting for the cam-
275 paign with a single parameters set.

276 We note that an absolute validation of the model and the pertinence of its long-term predic-
277 tions, requires confrontation with in-situ data over years of the cavern's lifetime. This can
278 be done when a continuous monitoring of the underground facilities is performed and in-situ
279 measurements are used to re-calibrate the model parameters and update the predictions.

280 **7. Acknowledgments**

281 This work has been performed in the framework of the projects CITEPH and STOPIL-
282 H2, the authors thank the sponsors and partners of the projects. The authors would also like
283 to acknowledge Michel Tijani from Mines ParisTech and Nicolas Gatelier from Geostock, for
284 their constructive discussions.

285 **References**

- 286 Bai, M., Song, K., Sun, Y., He, M., Li, Y., Sun, J., 2014. An overview of hydrogen underground stor-
287 age technology and prospects in China. *Journal of Petroleum Science and Engineering* 124, 132 –
288 136. URL: <http://www.sciencedirect.com/science/article/pii/S0920410514003374>, doi:<https://doi.org/10.1016/j.petrol.2014.09.037>.
289
- 290 Bays, C.A., 1963. Use of salt cavities for underground storage, in: *Symposium on Salt*. Northern Ohio
291 Geological Society., Cleveland, Ohio. pp. 564–578.
- 292 Bérest, P., Brouard, B., Karimi, M., Van Sambeek, L., 2007. Transient behaviour of salt caverns. In-
293 terpretation of mechanical integrity tests. *International Journal of Rock Mechanics and Mining Sci-*
294 *ences* 44, 767–786. URL: <http://www.sciencedirect.com/science/article/pii/S1365160906001894>,
295 doi:<https://doi.org/10.1016/j.ijrmms.2006.11.007>.
- 296 Bérest, P., Karimi, M., Brouard, B., 2008. Comportement mécanique à très long terme des mines et
297 cavernes dans le sel gemme : loi de Norton-Hoff ou loi de Lemaitre ? *Revue française de Géotechnique*
298 124. doi:[10.1051/geotech/2008124045](https://doi.org/10.1051/geotech/2008124045).
- 299 Deng, J., Liu, Y., Yang, Q., Cui, W., Zhu, Y., Liu, Y., Li, B., 2020. A viscoelastic, viscoplastic, and visco-
300 damage constitutive model of salt rock for underground energy storage cavern. *Computers and Geotech-*
301 *tics* 119, 103288. URL: <http://www.sciencedirect.com/science/article/pii/S0266352X19303520>,
302 doi:<https://doi.org/10.1016/j.compgeo.2019.103288>.
- 303 DeVries, K.L., Mellegard, K.D., Callahan, G.D., 2002. Salt damage criterion proof-of-concept research.
304 Technical Report RSI-1675 DE-FC26-00NT41026. RESPEC, Rapid city, South Dakota.
- 305 Firme, P.A., Roehl, D., Romanel, C., 2019. Salt caverns history and geomechanics towards future natural
306 gas strategic storage in Brazil. *Journal of Natural Gas Science and Engineering* 72, 103006. URL:
307 <http://www.sciencedirect.com/science/article/pii/S1875510019302586>, doi:[https://doi.org/](https://doi.org/10.1016/j.jngse.2019.103006)
308 [10.1016/j.jngse.2019.103006](https://doi.org/10.1016/j.jngse.2019.103006).
- 309 Gharbi, H., Bérest, P., Blanco-Martín, L., Brouard, B., 2020. Determining upper and lower bounds for
310 steady state strain rate during a creep test on a salt sample. *International Journal of Rock Mechan-*
311 *ics and Mining Sciences* 134, 104452. URL: [http://www.sciencedirect.com/science/article/pii/](http://www.sciencedirect.com/science/article/pii/S1365160920308212)
312 [S1365160920308212](http://www.sciencedirect.com/science/article/pii/S1365160920308212), doi:<https://doi.org/10.1016/j.ijrmms.2020.104452>.
- 313 Günther, R.M., Salzer, K., Popp, T., Lüdeling, C., 2015. Steady-state creep of rock salt: Improved ap-
314 proaches for lab determination and modelling. *Rock Mechanics and Rock Engineering* 48. doi:[10.1007/](https://doi.org/10.1007/s00603-015-0839-2)
315 [s00603-015-0839-2](https://doi.org/10.1007/s00603-015-0839-2).
- 316 Hampel, A., 2012. The CDM constitutive model for the mechanical behavior of rock salt: Recent develop-
317 ments and extensions, in: *Mechanical Behavior of Salt VII - Proceedings of the 7th Conference on the*
318 *Mechanical Behavior of Salt*, pp. 45–55.

319 Heusermann, S., Rolfs, O., Schmidt, U., 2003. Nonlinear finite-element analysis of solution mined stor-
320 age caverns in rock salt using the Lubby2 constitutive model. *Computers & Structures* 81, 629 –
321 638. URL: <http://www.sciencedirect.com/science/article/pii/S0045794902004157>, doi:[https://doi.org/10.1016/S0045-7949\(02\)00415-7](https://doi.org/10.1016/S0045-7949(02)00415-7). k.J Bathe 60th Anniversary Issue.
322
323 Iordache, I., Schitea, D., Gheorghe, A.V., Iordache, M., 2014. Hydrogen underground storage in Roma-
324 nia, potential directions of development, stakeholders and general aspects. *International Journal of*
325 *Hydrogen Energy* 39, 11071 – 11081. URL: <http://www.sciencedirect.com/science/article/pii/S0360319914014153>, doi:<https://doi.org/10.1016/j.ijhydene.2014.05.067>.
326
327 Julien, M., 1999. Une modélisation constutive et numérique du comportement rhéologique du sel gemme.
328 Ph.D. thesis. Ecole Polytechnique de Montréal.
329 Karimi-Jafari, M., 2007. Comportement transitoire des cavités salines profondes. Ph.d. thesis. Ecole Poly-
330 technique X.
331 Khaledi, K., Mahmoudi, E., Datcheva, M., Schanz, T., 2016. Stability and serviceability of underground
332 energy storage caverns in rock salt subjected to mechanical cyclic loading. *International Journal of*
333 *Rock Mechanics and Mining Sciences* 86, 115 – 131. URL: <http://www.sciencedirect.com/science/article/pii/S1365160916300612>, doi:<https://doi.org/10.1016/j.ijrmms.2016.04.010>.
334
335 Labaune, P., 2018. Comportement thermomécanique du sel gemme : Application au dimensionnement des
336 cavités. Ph.D. thesis. Mines ParisTech.
337 Labaune, P., Rouabhi, A., Tijani, M., Blanco-Martín, L., You, T., 2018. Dilatancy criteria for salt cavern
338 design: A comparison between stress- and strain-based approaches. *Rock Mechanics and Rock Engineering*
339 51, 599–611. doi:<https://doi.org/10.1007/s00603-017-1338-4>.
340 Lankof, L., Tarkowski, R., 2020. Assessment of the potential for underground hydrogen storage
341 in bedded salt formation. *International Journal of Hydrogen Energy* 45, 19479 – 19492. URL:
342 <http://www.sciencedirect.com/science/article/pii/S0360319920317523>, doi:<https://doi.org/10.1016/j.ijhydene.2020.05.024>.
343
344 Lord, A.S., Kobos, P.H., Borns, D.J., 2014. Geologic storage of hydrogen: Scaling up to meet city
345 transportation demands. *International Journal of Hydrogen Energy* 39, 15570 – 15582. URL:
346 <http://www.sciencedirect.com/science/article/pii/S0360319914021223>, doi:<https://doi.org/10.1016/j.ijhydene.2014.07.121>.
347
348 Michalski, J., Bünger, U., Crotogino, F., Donadei, S., Schneider, G.S., Pregger, T., Cao, K.K., Heide,
349 D., 2017. Hydrogen generation by electrolysis and storage in salt caverns: Potentials, economics and
350 systems aspects with regard to the German energy transition. *International Journal of Hydrogen Energy*
351 42, 13427 – 13443. URL: <http://www.sciencedirect.com/science/article/pii/S0360319917306109>,
352 doi:<https://doi.org/10.1016/j.ijhydene.2017.02.102>. Special Issue on The 21st World Hydrogen

353 Energy Conference (WHEC 2016), 13-16 June 2016, Zaragoza, Spain.

354 Munson, D., Dawson, P., 1981. Salt constitutive modeling using mechanism maps, in: First conference on
355 the mechanical behavior of salt, pp. 717–737.

356 Nazary Moghadam, S., Mirzabozorg, H., Noorzad, A., 2013. Modeling time-dependent behavior of gas
357 caverns in rock salt considering creep, dilatancy and failure. *Tunnelling and Underground Space Technol-*
358 *ogy* 33, 171 – 185. URL: <http://www.sciencedirect.com/science/article/pii/S0886779812001605>,
359 doi:<https://doi.org/10.1016/j.tust.2012.10.001>.

360 Odqvist, F.K.G., 1966. *Mathematical theory of creep and rupture*. Oxford University Press.

361 Ozarslan, A., 2012. Large-scale hydrogen energy storage in salt caverns. *International Journal of Hy-*
362 *drogen Energy* 37, 14265 – 14277. URL: [http://www.sciencedirect.com/science/article/pii/](http://www.sciencedirect.com/science/article/pii/S0360319912017417)
363 [S0360319912017417](http://www.sciencedirect.com/science/article/pii/S0360319912017417), doi:<https://doi.org/10.1016/j.ijhydene.2012.07.111>. hYFUSEN.

364 Rouabhi, A., Labaune, P., Tijani, M., Gatelier, N., Hévin, G., 2019. Phenomenological behavior of rock
365 salt: On the influence of laboratory conditions on the dilatancy onset. *Journal of Rock Mechanics and*
366 *Geotechnical Engineering* 11, 723 – 738. URL: [http://www.sciencedirect.com/science/article/](http://www.sciencedirect.com/science/article/pii/S1674775518304323)
367 [pii/S1674775518304323](http://www.sciencedirect.com/science/article/pii/S1674775518304323), doi:<https://doi.org/10.1016/j.jrmge.2018.12.011>.

368 Soubeyran, A., Rouabhi, A., Coquelet, C., 2019. Thermodynamic analysis of carbon dioxide stor-
369 age in salt caverns to improve the power-to-gas process. *Applied Energy* 242, 1090 – 1107. URL:
370 <http://www.sciencedirect.com/science/article/pii/S0306261919305112>, doi:[https://doi.org/](https://doi.org/10.1016/j.apenergy.2019.03.102)
371 [10.1016/j.apenergy.2019.03.102](https://doi.org/10.1016/j.apenergy.2019.03.102).

372 Tarkowski, R., Czapowski, G., 2018. Salt domes in Poland – potential sites for hydrogen
373 storage in caverns. *International Journal of Hydrogen Energy* 43, 21414 – 21427. URL:
374 <http://www.sciencedirect.com/science/article/pii/S0360319918331410>, doi:[https://doi.org/](https://doi.org/10.1016/j.ijhydene.2018.09.212)
375 [10.1016/j.ijhydene.2018.09.212](https://doi.org/10.1016/j.ijhydene.2018.09.212).

376 Tijani, M., Vouille, G., Hugout, B., 1983. Le sel gemme en tant que liquide visqueux, in: *International*
377 *congress on rock mechanics*, Melbourne, Australia. pp. 241–246.

378 Wolters, R., Lux, K., Düsterloh, U., 2012. Evaluation of rock salt barriers with respect to tightness:
379 Influence of thermomechanical damage, fluid infiltration and sealing/healing, in: *Proceedings of the 7th*
380 *international conference on the mechanical behavior of salt*, Paris, pp. 425–434.

381 Wu, F., Zhang, H., Zou, Q., Li, C., Chen, J., Gao, R., 2020. Viscoelastic-plastic damage creep model
382 for salt rock based on fractional derivative theory. *Mechanics of Materials* 150, 103600. URL:
383 <http://www.sciencedirect.com/science/article/pii/S0167663620306426>, doi:[https://doi.org/](https://doi.org/10.1016/j.mechmat.2020.103600)
384 [10.1016/j.mechmat.2020.103600](https://doi.org/10.1016/j.mechmat.2020.103600).